Phase diagram of coherently precessing states under superflow in ^{3}He-*B*

J. S. Korhonen and G. E. Volovik
Low Temperature Laboratory, Helsinki University of Technology, 02150, Espoo, Finland, and Landau Institute for Theoretical Physics, 117334 Moscow

Submitted 22 February 1992
Pis'ma Zh. Eksp. Teor. Fiz. **55**, No. 6, 358–362 (25 March 1992)

The phase diagram for the ordered *B*-phase states under the condition of the transverse NMR is constructed. Three phases, including the homogeneously precessing states, are separated by the first-order transition lines.

The coherent Larmor precession of magnetization in superfluid ^{3}He-*B* represents the time-dependent ordered state with the highest broken symmetry in condensed matter. The precessing state has a rigidity, which is the main feature of the ordered state with broken symmetry. This provides the high stability of coherent precession. Such anomalously stable coherent precession of magnetization (homogeneously precessing domain, HPD) was discovered in 1984 by the combined theoretical and experimental efforts,[1] and now is used in the experimental investigation of the intricate properties of the ^{3}He-*B* in the presence of superflow.[2,3] These experiments require a detailed knowledge of the interaction of the precessing state with the vortex cluster and the counterflow $\vec{v}_s - \vec{v}_n$ of the superfluid component and the normal component of the ^{3}He-*B* outside the cluster. The pioneering theoretical work on this subject is attributed to Bunkov and Timofeevskaya,[4] who investigated the structure of the domain boundary between the HPD and the nonprecessing domain (NPD) in the presence of the counterflow.

Here we discuss the domain boundaries from the general arguments of the first-order phase transition between different ordered states, which can exist in superfluid ^{3}He-*B* under conditions of the transverse NMR, i.e., when a small rf field with the frequency ω close to the Larmor frequency γH is applied perpendicular to the external field $\vec{H}$ (γ is the gyromagnetic ratio for ^{3}He nucleus, which we set to unity). We find the phase diagram between three ordered states (see Fig. 1): (i) HPD, (ii) NPD, and (iii) the precessing state, whose direction of magnetization is opposite to that of $\vec{H}$ (reversed spin domain, RSD). The first-order phase transitions between these states account for the existence of three domain boundaries: HPD-NPD, HPD–RSD, and NPD–RSD, whose position in the vessel can be stablized by application of the field or the velocity gradient. The structure of the HPD–NPD phase boundary within the vortex cluster and in the presence of the counterflow is discussed.

The Larmor precession of ^{3}He-*B* in the limiting case, where the dipole interaction is neglected, can be obtained from the initial stationary state, with the equilibrium magnetization $\vec{S}^{(0)} = \chi\vec{H}$ and orthogonal order parameter matrix $R^{(0)}$, by special symmetry operation, which comes from the Larmor theorem. According to the Larmor theorem, the effect of magnetic field on the spins of the ^{3}He atoms completely disappears in the system that rotates with the Larmor frequency. Therefore, the spin rota-

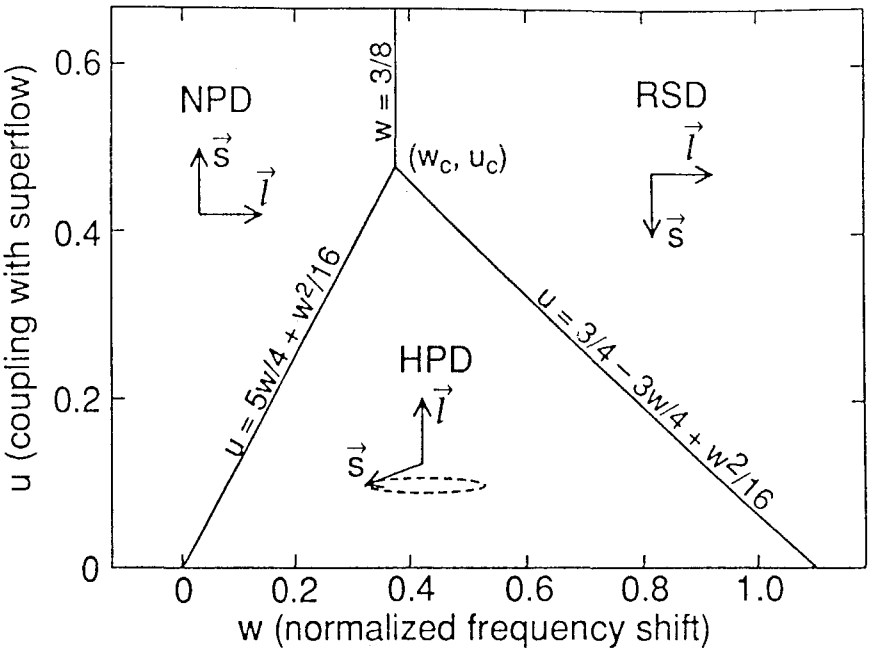

FIG. 1. Phase diagram for the coherent states. Except at the point $(u=0, w=0)$, the transitions are first-order transitions.

tion operation in the precessing frame does not change the energy of the system. If $R^{(p)}$ is the matrix of spin rotations in the precessing frame, it defines the orientation of the B-phase order parameter matrix $R_{\alpha i}(t)$ and magnetization $S_\alpha(t)$ for the general Larmor precession in the following way:

$$R_{\alpha i}(t) = O_{\alpha\beta}(\hat{z}, \omega t) R^{(p)}_{\beta\gamma} O_{\gamma\mu}(\hat{z}, -\omega t) R^{(0)}_{\mu i}, \quad S_\alpha(t) = O_{\alpha\beta}(\hat{z}, \omega t) R^{(p)}_{\beta\gamma} S^{(0)}_\gamma \quad , \quad (1)$$

where $O(\hat{z},\omega t)$ is the transformation from the laboratory frame into the rotating frame—this is the rotation about the z axis (along $\vec{H}$) by an angle ωt. Equation (1) means that to produce the symmetry transformation, one should first make the transformation from the laboratory frame into the precessing frame, then produce the $R^{(p)}$ rotation within this frame, and after that return to the laboratory frame.

The space of the degenerate states of the Larmor precession is larger than in the stationary state: In addition to the degeneracy parameter $R^{(0)}$, the Larmor precession is characterized by another time-independent matrix $R^{(p)}$. The physical meaning of these matrices is as follows: the $R^{(p)}$ matrix shows the orientation of the spin in the precessing frame according to Eq. (1), $S^{(p)}_\beta = R^{(p)}_{\beta\gamma} S^{(0)}_\gamma$. If $\hat{s}$ is the direction of magnetization in the precessing frame, then its projection onto $\vec{H}$ is $\hat{s}_z = R^{(p)}_{zz}$. The $R^{(0)}$ matrix shows the orientation $\vec{l}$ of the orbital momentum $L_i = -R_{\alpha i}(t) S_\alpha(t) = -R^{(0)}_{\alpha i} S^{(0)}_\alpha$, which is constant in the laboratory frame. If $\hat{l}_z$ is the z projection of $-\vec{l}$, we have $\hat{l}_z = R^{(0)}_{zz}$.

Three terms contribute to the energy of the coherently precessing state and lift the degeneracy. (i) After averaging over the period of precession, the dipole energy depends on only three degeneracy parameters.

$$F_D = \frac{2}{15}\chi\Omega_L^2[(\hat{s}_z\hat{l}_z - \frac{1}{2} + \frac{1}{2}\cos\gamma(1+\hat{s}_z)(1+\hat{l}_z))^2$$

$$+\frac{1}{8}(1-\hat{s}_z)^2(1-\hat{l}_z)^2 + (1-\hat{s}_z^2)(1-\hat{l}_z^2)(1+\cos\gamma)] \quad . \tag{2}$$

Here Ω_L is the Leggett frequency, and if one introduces the Euler angles for matrices $R = R_z(\alpha)R_y(\beta)R_z(\gamma)$, then $\gamma = \gamma^{(p)} - \gamma^{(0)}$. Note the symmetry between the spin and orbital vectors $\hat{s}$ and $-\hat{l}$ in the dipole energy.

(ii) The so-called spectroscopic term appears if the frequency of the rf field deviates from Larmor frequency. In this case the Zeeman energy $-\vec{H}\cdot\vec{S}$ is not compensated for completely by the Larmor energy of precession $\vec{\omega}\cdot\vec{S}$; therefore, one has the difference

$$F_\omega = (\vec{\omega} - \vec{H})\cdot\vec{S} = \chi\omega(\omega - H)\hat{s}_z \quad . \tag{3}$$

(iii) Typically under rotation of the vessel the vortex cluster appears at the center of the vessel which is separated by the vortex-free counterflow region from the side walls. Vortices and counterflow interact with the orbital anisotropy vector $\vec{l}$:[5]

$$F_{\text{counterflow}} = -\frac{1}{2}\rho_a((\vec{v}_s - \vec{v}_n)\cdot\hat{l})^2 \quad , \quad F_{\text{vortices}} = \lambda_{\text{vortices}}(\hat{\Omega}\cdot\hat{l})^2 \quad , \tag{4}$$

where $\hat{\Omega}$ is the direction of rotation.

The equilibrium states are obtained by the minimization of $F = F_D + F_\omega + F_{\text{vortices}}$ within the vortex cluster or $F = F_D + F_\omega + F_{\text{counterflow}}$ within the counterflow region. If $\hat{\Omega}\|\vec{H}$, both energies have the same structure:

$$\tilde{F} = u\hat{l}_z^2 + v\hat{s}_z + [(\hat{s}_z\hat{l}_z - \frac{1}{2} + \frac{1}{2}\cos\gamma(1+\hat{s}_z)(1+\hat{l}_z))^2$$

$$+\frac{1}{8}(1-\hat{s}_z)^2(1-\hat{l}_z)^2 + (1-\hat{s}_z^2)(1-\hat{l}_z^2)(1+\cos\gamma)] \quad , \tag{5}$$

where we have normalized the energy in terms of the dipole energy by introducing the dimensionless variables:

$$\tilde{F} = \frac{15F}{2\chi\Omega_L^2} \quad , \quad w = \frac{15\omega(\omega - H)}{2\Omega_L^2} \quad ,$$

$$u = \frac{15\rho_a(\vec{v}_s - \vec{v}_n)^2}{4\chi\Omega_L^2} \quad \text{or} \quad u = \frac{15\lambda_{\text{vortices}}}{2\chi\Omega_L^2} \quad . \tag{6}$$

Minimization shows that there are three competing states: (i) Nonprecessing state (NPD) with $\hat{s}_z = 1$, $\hat{l}_z = 0$ and $\cos\gamma = 1/2$; (ii) HPD with $\hat{l}_z = 1$ and $\cos\gamma = 1$,

the precessing magnetization is tilted by angle $\cos\beta = \hat{s}_z = \frac{1}{4} - \frac{w}{8}$; and (iii) the precessing state with the reversed spin (RSD): $\hat{s}_z = -1$, $\hat{l}_z = 0$, while γ is arbitrary. This state differs from the periodic solution with $\hat{s}_z = -1$, which is discussed by Fomin,[6] by orientation of $\hat{l}$, and therefore has different stability condition. The energies of these states are

$$\tilde{F}_{\mathrm{NPD}} = w \quad , \quad \tilde{F}_{\mathrm{HPD}} = u - \frac{1}{4}w - \frac{1}{16}w^2 \quad , \quad \tilde{F}_{\mathrm{RSD}} = -w + \frac{3}{4} \quad , \tag{7}$$

and the phase diagram in the w,u plane contains the triple point $w_c = \frac{3}{8}$, $u_c = \frac{489}{1024}$, where the three first-order transition lines merge (see Fig. 1).

The transition line between HPD and NPD, at which $F_{\mathrm{HPD}} = F_{NPD}$,

$$u = \frac{5}{4}w + \frac{1}{16}w^2 \quad , \tag{8}$$

represents the first-order phase transition, except at the point $w = 0$, $u = 0$. The first-order transition line between RSD and NPD, $w = \frac{3}{8}$, exists at $u > u_c$. The first-order transition line between HPD and RSD, $u = \frac{3}{4} - \frac{3}{4}w + \frac{1}{16}w^2$, exists at $u < u_c$, $w > w_c$ and gives rise to the domain boundary between HPD and RSD (Fig. 2). Because of the nature of the first-order phase transitions, the metastability is possible. The HPD state is metastable in the regions of the NPD or RSD stability until it becomes absolutely unstable at $u = \frac{15}{8} - \frac{3}{32}\omega - \frac{5}{64}w^2$. Above this line, the instability toward the deviation of $\hat{l}$ from the $\hat{z}$ direction develops. The instability of the NPD toward RSD develops at $w > 3$, it starts with the deviation of $\hat{s}$ from the $\hat{z}$ direction. The instability of RSD

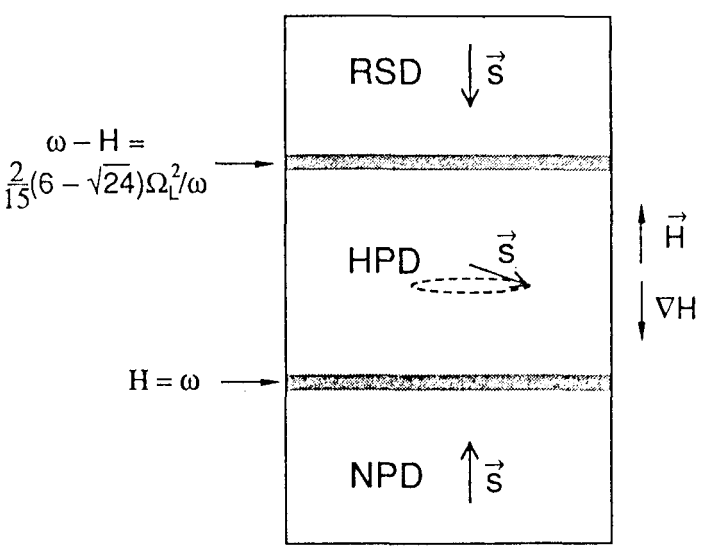

FIG. 2. Three-domains precession in a large field gradient along z; $0 \leqslant u < u_c$. In the absence of the counterflow ($u = 0$), the positions z_1 and z_2 of the domain boundaries are defined by $H(z_1) = w$ for HPD–NPD boundary and $w - H(z_2) = \frac{2}{13}(6 - \sqrt{24})\Omega_L^2/w$ for the HPD–RSD boundary.

toward NPD develops at $w<0$. We also found another metastable local minimum of Eq. (5) with $\hat{l}_z = -1$ and $\hat{s}_z = -\frac{w}{3}$. Let us now consider the core structure of the domain boundary between HPD and NPD. The simplest structure is obtained in the limit of the infinitely large dipole energy, compared to the interaction with the counterflow or with the vortex cluster. From minimization of Eq. (2) it follows that at each point of space, including the core of the domain boundary, one has either $\hat{s}_z = 1$, i.e., the nonprecessing state described by the single matrix $R^{(0)}(\hat{n},\theta_0)$, or $\hat{l}_z = 1$ which corresponds to the HPD state described by the single matrix $R^{(p)}(\hat{n},\theta_0)$. Both matrices are parametrized by the $\hat{n}$ axis of rotation by the magic angle $\cos\theta_0 = -1/4$ of rotation, which is fixed by the dipole energy. At the interface between these regions $\hat{n}\|\vec{H}$: it is the only way to match the precessing $\hat{n}$ on the HPD side with the stationary $\hat{n}$ on the NPD side. According to Eq. (8), this interface is positioned within the counterflow region at the place where $\frac{5}{4}\chi\omega(\omega - H) = \frac{1}{2}\rho_a(\vec{v}_s - \vec{v}_n)^2$, and within the vortex cluster at the place where $\frac{5}{4}\chi\omega(\omega - H) = \lambda_{\text{vortices}}$.

Since F_ω orients the $\hat{n}$ vector perpendicular to the magnetic field well inside the HPD region, and $F_{\text{counterflow}}$ or $F_{vortices}$ orients $\hat{l}$ perpendicular to the magnetic field deep inside the NPD, which corresponds to $n_z^2 = 1/5$, the $\hat{n}$ texture appears on both sides of the interface. To find the texture, one should minimize the orientation energy on each side of the interface, together with the gradient energy F_g, using the boundary condition $\hat{n}\|\vec{H}$ at the interface. In the geometry, where the phase boundary is perpendicular to $\vec{H}$, F_g has the same form in terms of the $\hat{n}$ vector for each texture

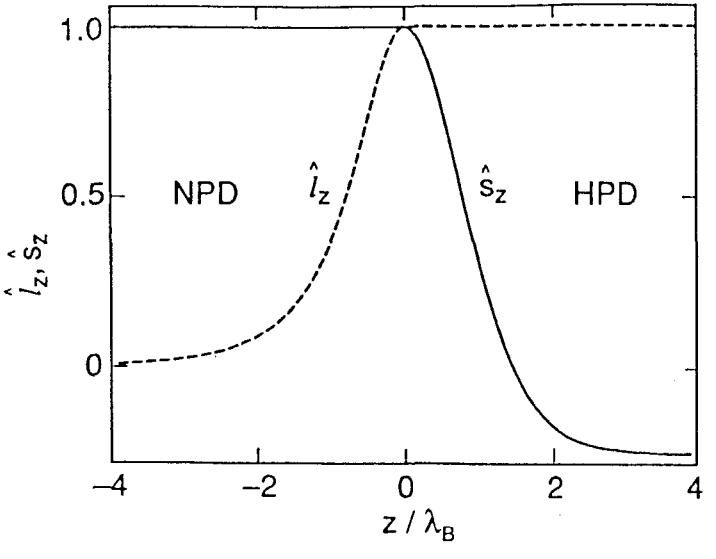

FIG. 3. The structure of the HPD–NPD boundary in the presence of vortices or counterflow for particular case $c_\perp = \sqrt{2}c_\parallel$, which holds near T_c. Dashed line—The profile of $\hat{l}_z$, solid line—$\hat{s}_z$. The length is scaled in terms of $\lambda_B = c_\perp/\sqrt{w(w - H(z_1))} = \sqrt{3/u}\,c_\perp/\Omega_L$, which was introduced in Ref. 4.

$$F_g = \chi c_\perp^2 (1 - \cos\theta_0)(\partial_i \hat{n})^2$$
$$- \frac{1}{2}\chi(c_\perp^2 - c_\parallel^2)(\sin\theta_0 \vec{\nabla}\cdot\hat{n} + (1-\cos\theta_0)\hat{n}\cdot\vec{\nabla}\times\hat{n})^2 \quad , \tag{9}$$

where $c_\parallel$ and $c_\perp$ are longitudinal and transverse spin wave velocities [these are related to the Fomin definition[6]: $c^2_{\parallel\,\mathrm{Fomin}} = c_\perp^2$ and $c^2_{\perp\,\mathrm{Fomin}} = (1/2)(c_\perp^2 + c_\parallel^2)$].

The texture on the HPD side (Fig. 3) does not depend on what occurs in the NPD region and coincides with it.[4] The NPD texture depends on the type of the orientational energy in Eq. (4). Figure 3 shows the $\hat{l}_z$ texture which takes place within the vortex cluster, while the NPD texture in the counterflow region is slightly different due to violation of the axial symmetry by the fixed direction of the counterflow in the transverse plane. Our NPD texture is essentially smoother than that in Ref. 4, where the gradient energy on the NPD side was disregarded. At $0 < u < u_c$ both $\hat{n}$ textures, which together comprise the core of the phase boundary between HPD and NPD, have internal thickness $\sim u^{-1/2} c_\perp/\Omega_L$, which diverges as $u \to 0$: at $u = 0$ the thickness of HPD–NPD domain boundary is determined by the magnitude of the magnetic field gradient.[1]

So far, experiments were concentrated in the region of small w, where only the HPD–NPD boundary was investigated. We suggest that the region of w be extended to observe the other domain boundaries.

We wish to thank Yu. M. Bunkov, V. V. Dmitriev, M. Krusius, T. Sh. Misirpashaev, and E. Thuneberg for discussions. This work was supported by the ROTA cooperation project between the Academy of Finland and the USSR Academy of Sciences.

[1]A. Borovik-Romanov, Yu. Bunkov, V. Dmitriev, and Yu. Mukharsky, Pis'ma Zh. Eksp. Teor. Fiz. **40**, 256 (1984) [JETP Lett. **40**, 1033 (1984)]; I. A. Fomin, Pis'ma Zh. Eksp. Teor. Fiz. **40**, 260 (1984) [JETP Lett. **40**, 1037 (1984)].
[2]Yu. M. Bunkov and P. J. Hakonen, J. Low. Temp. Phys. **83**, 323 (1991).
[3]Y. Kondo, J. S. Korhonen, M. Krusius *et al.*, Phys. Rev. Lett. **67**, 81 (1991).
[4]Yu. Bunkov and O. Timofeevskaya, Pis'ma Zh. Eksp. Teor. Fiz. **54**, 232 (1991) [JETP Lett. **54**, 228 (1991)].
[5]P. J. Hakonen, M. Krusius, M. M. Salomaa *et al.*, J. Low Temp. Phys. **76**, 225 (1989).
[6]I. A. Fomin, in *Modern Problems in Condensed Matter Sciences, Vol. 26, Helium Three,* W. P. Halperin and L. P. Pitaevskii, Eds. (North-Holland, 1990), p. 610.

Translated by the authors